Zeolitic Imidazolate Framework Nanoencapsulation of CpG for Stabilization and Enhancement of Immunoadjuvancy

Olivia R. Brohlin, Ryanne N. Ehrman, Fabian C. Herbert, Yalini H. Wijesundara, Arun Raja, Arezoo Shahrivarkevishahi, Shashini D. Diwakara, Ronald A. Smaldone, and Jeremiah J. Gassensmith†*

Department of Chemistry and Biochemistry, The University of Texas at Dallas, 800 W. Campbell Road, Richardson, Texas 75080, United States

†Department of Biomedical Engineering, The University of Texas at Dallas, 800 W. Campbell Road, Richardson, Texas 75080, United States

*E-mail: gassensmith@utdallas.edu. Web: www.gassensmithlab.com

KEYWORDS

Metal-organic framework, zeolitic imidazolate framework 8, CpG, immunoadjuvant, phosphodiester DNA, B-cell activation, nuclease resistance

ABSTRACT

Metal organic frameworks (MOFs) have been used to improve vaccine formulations by stabilizing proteins and protecting them against thermal degradation. This has led to increased

immunogenicity of these proteinaceous therapeutics. In this work we show that MOFs can also be used to protect the ssDNA oligomer, CpG, to increase its immunoadjuvancy. By encapsulating phosphodiester CpG in the zinc-based MOF, ZIF-8, the DNA oligomer is protected from nuclease degradation and exhibits improved cellular uptake. As a result, we have been able to achieve drastically enhanced B-cell activation in splenocyte cultures comparable to the current state-of-the-art, phosphorothioate CpG. Furthermore, we have made a direct comparison of micro- and nano-sized MOF for the optimization of particulate delivery of immunoadjuvants to maximize immune activation.

INTRODUCTION

Metal organic frameworks (MOFs) have been used to stabilize a wide variety of biomacromolecules including proteins,[1-2] viruses,[3] and liposomes[4] against thermal degradation as a means to overcome the "Cold Chain". This technology has been revolutionary in overcoming the notorious instability of biological therapeutics and offers the possibility of significantly reducing their cost and increasing their accessibility – specifically in developing areas that lack the infrastructure to maintain the required refrigeration for storage and transport.[5-6] These powerful polymeric frameworks are formed through coordination bonds between a metal node and organic linkers.[7-9] Biomacromolecules act as nucleating agents that catalyze MOF formation, resulting in encapsulation through a process called biomimetic mineralization.[10-13] Once encapsulated, the biomacromolecule is protected from enzymatic degradation[14] and thermal denaturation.[15-16] The resulting structure is thermodynamically stable[17-19] but is kinetically labile and easily degrades in the presence of strong metal chelators,[20-21] low pH,[22-23] and inorganic phosphates[24] that allows for the recovery of the preserved biomacromolecule. In this work, we

apply this technology for the encapsulation of the single stranded DNA (ssDNA) immunoadjuvant, CpG.

Vaccines often have a limited ability to activate the B- and T-cell mediated components of the immune system and therefore must be combined with an immunoadjuvant to promote and direct the immune response.[25-27] Synthetic adjuvants designed to mimic pathogen-associated molecular patterns (PAMPs) can bind to pattern recognition receptors (PRRs) to begin the process of switching immune cells from a passive naïve state to an active state ready to fight infection.[28-29] CpG is a synthetic immunoadjuvant composed of single stranded, unmethylated, bacterial DNA.[30-31] In mammals, 70-80% of CpG cytosines are methylated, therefore unmethylated CpG is recognized by the immune system as a PAMP.[32-33] The immunoadjuvant, CpG, can activate both plasmacytoid dendritic cells (pDCs) and B-cells to trigger a proinflammatory response.[34] This is important as pDCs are the body's vanguards against infection by foreign pathogens and proliferation of cancer while B-cells are responsible for producing different types of proteins that bind to and neutralize infection – in particular different types of immunoglobulins or antibodies.

There are two main types of CpG, each specializing in activating a specific part of the innate immune system. Class A CpG (also referred to as D-type) more strongly activates pDCs and promotes a T cell mediated cellular immune response;[35] whereas, class B CpG (K-type) more strongly activates B-cells and promotes a humoral immune response.[36] Due to it's ability to boost antibody production, class B CpG immunoadjuvants have been the focus of human clinical trials for vaccines, infectious diseases, and cancer.[37-39] The major limitation undermining the success of CpG in clinical trials comes from the nuclease susceptibility of the DNA backbone.[40] The current state-of-the-art technology has reengineered the labile phosphodiester (PO)

backbone by thiolation of the sugar moiety to form a nuclease-resistant phosphorothioate (PS) bond, resulting in an increased *in vivo* half-life of 30–60 min (5–10 min for PO).[41] However, this modification has been found to lower the immunoadjuvancy of CpG and induce acute toxicity.[42-43]

As an alternative to the PS backbone modification, we propose using MOFs to improve the *in vivo* stability of PO CpG. In this way, we can protect CpG from nucleases while also retaining the innate immunoadjuvancy of the oligonucleotide. Recent work with zeolitic imidazolate framework-8 (ZIF-8), a zinc-based MOF, has shown it possible to grow a MOF shell around biomacromolecules in a simple one-pot synthesis under ambient conditions.[44-47] The resulting formulation does not require refrigeration, unlike other currently used nanocarriers such as lipid nanoparticles,[48] virus-like particles,[49] and liposomes.[50] ZIF-8 forms a protective barrier that inhibits enzymatic degradation of biomacromolecules.[51] ZIF-8 has previously served[52] as a nanoparticle carrier of PS CpG by electrostatically binding the negatively charged CpG onto the cationic surface of the crystals to promote cellular uptake and enhance immunoadjuvancy in macrophages. In this work, we encapsulate PO CpG within ZIF-8 to protect the DNA from nucleases and enhance immunoadjuvancy by improving B-cell activation (**Scheme 1**). Furthermore, we have optimized our formulation by tuning the ZIF-8 metal-to-ligand ratios to synthesize both micro- and nano-sized CpG@ZIF.

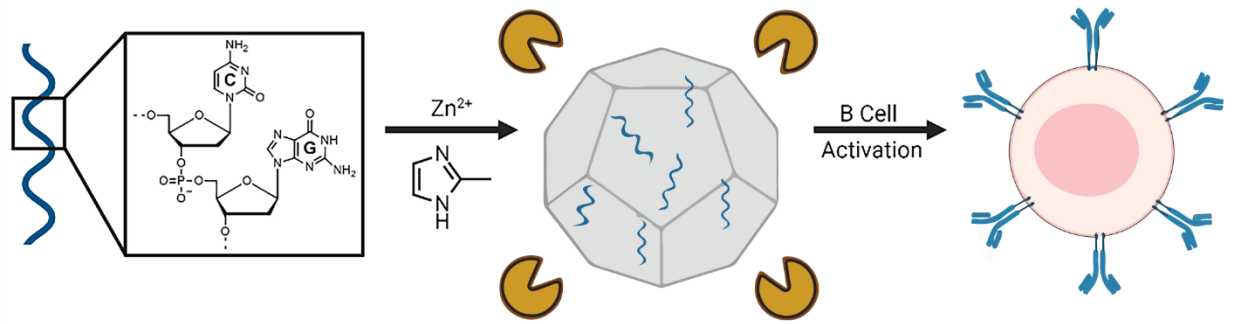

Scheme 1. Illustration of the encapsulation of CpG in ZIF-8 for enhanced immunoadjuvancy. The ssDNA immunoadjuvant, CpG, is encapsulated in the zinc-based MOF, ZIF-8, by biomimetic mineralization using Zn^{2+} and 2-methylimidazole. Encapsulation of CpG within ZIF-8 affords nucleic acid protection from nucleases and promotes cellular uptake for enhanced B-cell activation.

EXPERIMENTAL

Materials

PO CpG (ODN 1826-Class B) and FITC-labeled PO CpG were purchased as a custom DNA oligomer from Invitrogen (sequence: 5'-tccatgacgttcctgacgtt-3' (20 mer); 5' FAM modification). PS CpG (ODN 1826), FITC-labeled PS CpG (ODN 1826 FITC), and PS GpC (ODN 1826 control: ODN 2138) were purchased from Invivogen. Nuclease-free water, zinc acetate dihydrate, 2-methylimidazole, β-mercaptoethanol, RPMI-1640, Dulbecco's Modified Eagle Medium, FB Essence, penicillin-streptomycin, phosphate buffered saline, and Desoxyribonuclease I (DNase I) were purchased from Sigma-Aldrich (St. Louis, MO, USA), Thermo Fisher Scientific (Waltham, MA, USA), or VWR (Radnor, PA, USA). LDH-Cytox assay kit, cell staining buffer, RBC lysis buffer, Alexa Fluor® 700 anti-mouse CD19 Antibody, Alexa Fluor® 647 anti-mouse CD80 Antibody, and PE anti-mouse CD86 Antibody were purchased from Biolegend.

CpG@ZIF Synthesis and Characterization

Synthesis of CpG@ZIF

Stock solutions of 1 M $Zn(OAc)_2$ and 3 M 2-methylimidazole (HMIM) were made in nuclease-free water. For the synthesis of the CpG@μZIF, 213 μL of 3 M HMIM (final concentration 640 mM) was combined with 708 μL of nuclease-free water. 39 μL of 100 μM PO CpG (final concentration 25 μg/mL) was added and the solution was vortexed for 10 s. Lastly, 40 μL of 1 M $Zn(OAc)_2$ (final concentration 40 mM) was added and the solution was vortexed for another 30 s. The solution immediately turned turbid and was allowed to react at RT for 1 h. The same was done for the synthesis of CpG@nZIF using 853 μL of 3 M HMIM (final concentration 2560 mM), 28 μL nuclease-free water, 39 μL of 100 μM PO CpG (final concentration 25 μg/mL), and 80 μL 1 M $Zn(OAc)_2$ (final concentration 80 mM). For the synthesis of pristine ZIF, the same conditions were used except 39 μL of additional nuclease-free water was added in place of 39 μL of PO CpG. The resulting solutions were centrifuged at 17,000 ×*g* for 10 mins to obtain a pellet of the crystals. The crystals were then washed with 1000 μL of methanol, 500 μL methanol and 500 μL nuclease-free water mixture, and 1000 μL nuclease-free water using the same centrifugation method. The final pellet was resuspended in nuclease-free water. The same procedure was used for the encapsulation of FITC-labeled CpG. For adsorption of CpG onto the surface of ZIF (CpG+ZIFs), 39 μL of 100 μM PO CpG was combined with pristine ZIF in a total reaction volume of 100 μl and incubated on a rotisserie for 1 h at RT. The samples were purified by centrifugation (17,000 ×*g* for 10 mins) however no subsequent washings were employed to prevent dislodging the surface adsorbed CpG.

Characterization of CpG@ZIF

SEM. The surface morphology of the CpG@ZIFs was examined using a Zeiss Supra 40 scanning electron microscope at 2.5 kV and 6–10 mm working distance. 5 μL of the prepared crystals in nuclease free water were loaded onto a silicon wafer, allowed to dry for 10 s, and the excess

wicked off using Whatman Filter Paper #1. The samples were then sputtered with a ~40 Å layer of gold before being imaged.

DLS. The size and polydispersity of the CpG@ZIFs was quantified using a Malvern Analytical Zetasizer Nano ZS. 1 mL of the crystals diluted in nuclease-free water was loaded into a 1 mL disposable cuvette and read at 25 ºC, a 175º scattering angle, a medium refractive index of 1.33, a 633 nm laser, and a material refractive index of 1.51.

ζ Potential. The charge of the CpG@ZIFs was quantified using a Malvern Analytical Zetasizer Nano ZS. 1 mL of the crystals diluted in nuclease-free water was loaded into a 1 mL disposable folded capillary cell and read at 25 ºC.

PXRD. Crystallinity of the CpG@ZIFs was determined with a Rigaku SmartLab X-ray Diffractometer with CuKα (1.54060 Å) at 30 mA and 40 kV. The samples were washed with methanol and put under vacuum overnight before being analyzed.

BET Nitrogen Isotherms. The surface areas of the CpG@ZIFs were quantified using a Micrometrics ASAP 2020 surface area analyzer. Nitrogen adsorption measurements were taken at 77 K. Samples were activated in MeOH for 4 h, dried under vacuum for 24 h, soaked with DCM for 4 h, and finally dried under vacuum for another 24 h. Before analysis, the samples were put under vacuum and degassed at 120 °C for 12 h. The data was processed by Brunauer–Emmett–Teller (BET) method for calculation of the surface area and pore sizes quantified by a non-localized density functional theory (NLDFT) with a carbon slit pore model.

Confocal Microscopy. The fluorescence of the FITC-labeled PO CpG encapsulated in ZIF-8 was qualitatively observed using an Olympus FV3000 RS Confocal microscope. 10 µL of sample was loaded onto a glass slide, covered with a glass cover slip and left to dry overnight in the

dark. The slide was then sealed and imaged using 100 × magnification. Images were processed using ImageJ software.

Fluorimetry. The encapsulation efficiency of FITC-labeled PO CpG in ZIF-8 before and after denaturing washes was quantified by measuring the FITC fluorescence intensity of the supernatant during synthesis. For washing, CpG@ZIFs were either treated with 10% SDS for 30 mins at RT or 2 units of DNase I for 10 mins at 37 ºC. After, the solution was centrifuged at 17,000 ×*g* for 10 mins and 100 µL of the supernatant was added to a black 96 well plate in triplicate. Fluorescence readings at λ_{ex} = 495 nm; λ_{em} = 520 nm were performed on a BioTek Synergy H4 Hybrid Microplate Reader. The encapsulation efficiency was calculated as a percent of the FITC fluorescence intensity of the starting material.

CpG@ZIF Stability Against DNase I

The digestion was performed according to the manufacturer's protocol. In brief, 10 µg of encapsulated and unencapsulated PO CpG (as well as PS CpG) were incubated with 1 µL (2 units) of DNase I and 10 µL of 10× DNase reaction buffer (final concentration 1×) in a final reaction volume of 100 µL using nuclease-free water. The mixture was incubated for 10 mins at 37 ºC. The reaction was quenched with 1 µL of 0.5 M EDTA. The digested and undigested CpG@ZIFs samples were centrifuged at 17,000 ×*g* for 10 mins and the supernatants decanted. 100 µL of 0.5 M EDTA was used to dissolve the ZIF-8 crystals and recover the CpG. The recovered CpG samples were run on a 5% agarose gel containing 0.5 mg/mL ethidium bromide at 100 V for 10 mins with 1× TBE running buffer alongside a ultra low range DNA ladder. The same was done for adsorbed samples (CpG+ZIFs) except EDTA exfoliation was not required to recover the CpG.

CpG@ZIF Performance *In Vitro*

Cytotoxicity

The cell viability assay was performed according to the manufacturer's protocol. In brief, RAW 264.7 murine macrophages were grown in DMEM supplemented with 10% FB Essence and 1% penicillin-streptomycin. The cells were then seeded at a concentration of 1×10^6 cells/mL in a 96 well plate (100 µL/well) and allowed to adhere overnight. All incubations took place in a 37 °C CO_2 incubator. The following day the cells were treated with the CpGs, CpG@ZIFs, or ZIFs at a CpG concentration of 3.3 µg/mL (100 µL/well) for 4 h. Next, 10 µL of lysis buffer was added to a set of untreated cells for 30 mins to create the negative control. After, 100 µL of working solution was added to all of the wells for 30 mins in a light protected area. Lastly, 50 µL of stop solution was added to all wells before reading the absorbance at 490 nm on a BioTek Synergy H4 Hybrid Microplate Reader.

Uptake

Spleens from naïve BALB/c mice were collected from euthanized mice in accordance with protocol #19-06 approved by the University of Texas at Dallas Institutional Animal Care and Use Committee (IACUC). Spleens were homogenized into single cell suspensions using cell pestles and 100 µm cell strainers and red blood cells were lysed with 1× RBC lysis buffer. Splenocytes were seeded at 1×10^6 cells/mL in a 24 well plate (2 mL/well). The splenocytes were treated with FITC-labeled CpGs, CpG@ZIFs, or ZIFs (3.3 µg/mL CpG concentration) in RPMI supplemented with 10% FB Essence, 1% penicillin-streptomycin, and 50 µM β-mercaptoethanol for 4 h at 37 °C in a CO_2 incubator. After, the cells were washed 3× with 0.5 M sodium acetate buffer pH 5 to remove surface bound material, washed 3× with 1× PBS, stained

with Alexa Fluor® 700 anti-mouse CD19 Antibody to identify B cells, washed 3× with cell staining buffer, and finally resuspended in 1 mL of cell staining buffer. Quantitative analyses were completed using a BD LSR Fortessa flow cytometer with approximately 100,000 events collected per sample. Data processing was performed on FlowJo software Version 10.6.1.

B-cell Activation

Spleens from naïve BALB/c mice were collected from euthanized mice in accordance with protocol #19-06 approved by the University of Texas at Dallas Institutional Animal Care and Use Committee (IACUC). Spleens were homogenized into single cell suspensions using cell pestles and 100 μm cell strainers and red blood cells were lysed with 1× RBC lysis buffer. Splenocytes were seeded at 1×10^6 cells/mL in a 24 well plate (2 mL/well). The splenocytes were treated with FITC-labeled CpGs, CpG@ZIFs, or ZIFs (3.3 μg/mL CpG concentration) in RPMI supplemented with 10% FB Essence, 1% penicillin-streptomycin, and 50 μM β-mercaptoethanol for 4 h at 37 °C in a CO_2 incubator. The cells were washed 3× with 0.5 M sodium acetate buffer at pH 5 to remove surface bound material, washed 3× with 1× PBS, stained with Alexa Fluor® 700 anti-mouse CD19 Antibody, Alexa Fluor® 647 anti-mouse CD80 Antibody, and PE anti-mouse CD86 Antibody to identify activated B cells, washed 3× with cell staining buffer, and finally resuspended in 1 mL of cell staining buffer. Quantitative analyses were completed using a BD LSR Fortessa flow cytometer with approximately 100,000 events collected per sample. Data processing was performed on FlowJo software Version 10.6.1.

RESULTS AND DISCUSSION

Biomimetic mineralization of ZIF-8 on the surface of CpG was done by iteratively adjusting aqueous solutions of zinc acetate and 2-methylimidazole (HMIM) as the metal node

and organic ligand, respectively. Tuning the metal-to-ligand ratio allows us to not only capture the oligonucleotide, but also control the size of the ZIF-8. From our initial screen we found that we could produce CpG encapsulated in micro-sized crystals (CpG@μZIF) when we used 40 mM $Zn(OAc)_2$, 640 mM HMIM, and 25 μg/mL CpG. Further, we found that when we used 80 mM $Zn(OAc)_2$, 2560 mM HMIM, and 25 μg/mL CpG we could synthesize nano-sized crystals (CpG@nZIF). Prior work using[4] time-resolved X-ray spectroscopy shows ZIF-8 formation begins within seconds; consequently, the time the DNA resides at these high concentrations of metals and ligand is extremely short before it becomes encapsulated. SEM micrographs of the resulting micro (**Figure 1A**) and nano (**Figure 1B**) crystals show the characteristic rhombic dodecahedral shape of ZIF-8 that are consistent with pristine ZIFs (**Figure 1C&D**). Furthermore, the crystallinity of the CpG@ZIFs was measured by PXRD with the patterns matching that of pristine and simulated ZIF-8 (**Figure 1E**). Following activation, we found the resulting composites were still porous. As expected, the nitrogen isotherms of the CpG@μZIF and CpG@nZIF show diminished surface areas, which is attributed to the presence of CpG in the ZIF-8 (**Figure 1F**). The hydrodynamic radius of the resulting composites was measured via dynamic light scattering (DLS). From these data we found CpG@μZIF to have a size around ~1.3 μm (PDI: 0.374) whereas CpG@nZIF was ~215 nm (PDI: 0.470) (**Figure 1G**). The ability to control the size of the composites is important in the formulation of vaccines and adjuvants. Polymeric vaccine formulations often advocate for a larger particle size ranging from 500 nm to several microns with the advantage of providing a sustained release system.[53] With these constructs, we have seen a heightened humoral immune response and prolonged immunity, however, literature reports that particles should be less than 500 nm for optimal uptake by immune cells.[54-55] Having two sizes of CpG@ZIF both above and below this cut off allows us to

make a direct comparison of micro- and nano-size MOFs for optimal delivery of CpG and subsequent activation of B-cells. Further characterization of both micro and nano formulations found that encapsulation of the CpG in ZIF-8 resulted in a slight shielding of the strong negative charge of the DNA by the positively charged MOF (**Figure 1H**). It was hypothesized that this factor may also play an important role in mediating cell uptake as mammalian cell membranes are negatively charged owing to the presence of phosphatidyl serine and thus cargo with strong negative charges are thought to be electrostatically repelled from cell surfaces.[56-57]

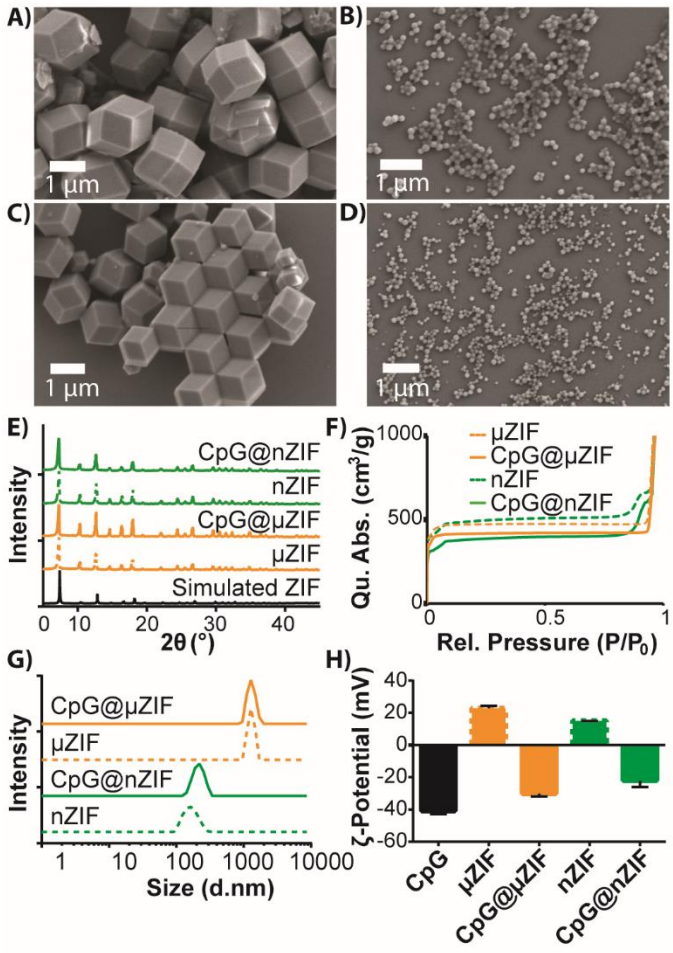

Figure 1. Encapsulation of CpG and in micro and nano ZIF-8. A) SEM micrograph of CpG@µZIF. B) SEM micrograph of CpG@nZIF. C) SEM micrograph of pristine µZIF. D) SEM

micrograph of pristine nZIF. E) PXRD patterns of CpG@μZIF and CpG@nZIF as compared to pristine and simulated ZIF-8. F) Brunauer–Emmett–Teller nitrogen isotherms assessing the reduction in surface area as a result of CpG encapsulation in μZIF and nZIF. G) DLS characterization of the size distribution of CpG@μZIF and CpG@nZIF. H) ζ-potential measurements illustrating the reduction in negative charge of CpG after encapsulation in the positively charged ZIFs.

To quantitatively and qualitatively confirm DNA encapsulation within ZIF, fluorescently-labeled CpG, FITC-CpG, was used. The encapsulation efficiency was first quantified by measuring the amount of unencapsulated material in the supernatant during synthesis. Fluorometric analyses shows that CpG was encapsulated quantitatively (~95%; 23-24 μg of CpG per mL of ZIF) in both sizes of ZIF (**Figure 2A&B**) — an important observation given the high cost of CpG. Qualitatively, confocal images of the micro and nano formulations found that the crystals were obviously fluorescent in the FITC channel (**Figure 2C**). Furthermore, SDS (**Figure 2D**) and DNase (**Figure 2E**) washes were employed to remove any surface bound material. From these experiments we note that nZIF seems to adsorb CpG onto the surface more than the larger μZIF, a phenomenon previously detailed by Li *et al*.[58] Given the high concentrations of metal and ligand, we were concerned that hydrolysis of the DNA backbone may occur. Curiously, ZIF growth has never been shown to degrade any biomacromolecules, even with such high concentrations of Lewis acids and alkaline ligands. To the contrary, ZIF shells grow and protect even very delicate systems like protein-embedded liposomes,[4] enzymes,[59-60] whole yeast,[61-62] and bacteria.[46, 63] To confirm that the CpG was not damaged during encapsulation, the ZIF shells of CpG@μZIF and CpG@nZIF were removed by treatment with 0.5 M EDTA to pull the Zn^{2+} from the coating and recover the DNA. Using a 5% agarose gel stained with ethidium bromide,

we found that the CpG was unaltered (**Figure 2F**). After confirming the CpG was properly encapsulated in the ZIF-8, we sought to test the ability of ZIF to protect CpG for nuclease degradation. We subjected both CpG@μZIF and CpG@nZIF, as well as CpG controls, to DNase I digestion. After incubation with DNase I for 10 mins at 37 ºC, the CpG@ZIFs samples were exfoliated using 0.5 M EDTA to remove the ZIF shell. The recovered CpG was run on a 5% agarose gel and visualized with ethidium bromide (**Figure 2F**). It was found that DNase I degraded the unencapsulated CpG whereas encapsulated CpG and PS CpG remained intact. This confirms that ZIF successfully protects CpG for nucleases. Furthermore, we tested CpG adsorbed onto the surface of ZIF (CpG+ZIF) to confirm that the nuclease protection was truly due to encapsulation of the CpG within the ZIF (**Figure 2F**). Mere surface adsorption did not provide the same protection as encapsulation with complete degradation of the CpG observed following treatment of CpG+ZIF with DNase I. In addition, it was noted that CpG was adsorbed to the surface of nZIF more strongly than μZIF as made evident by the reduced electrophoretic mobility of the CpG, which corroborates our earlier findings.

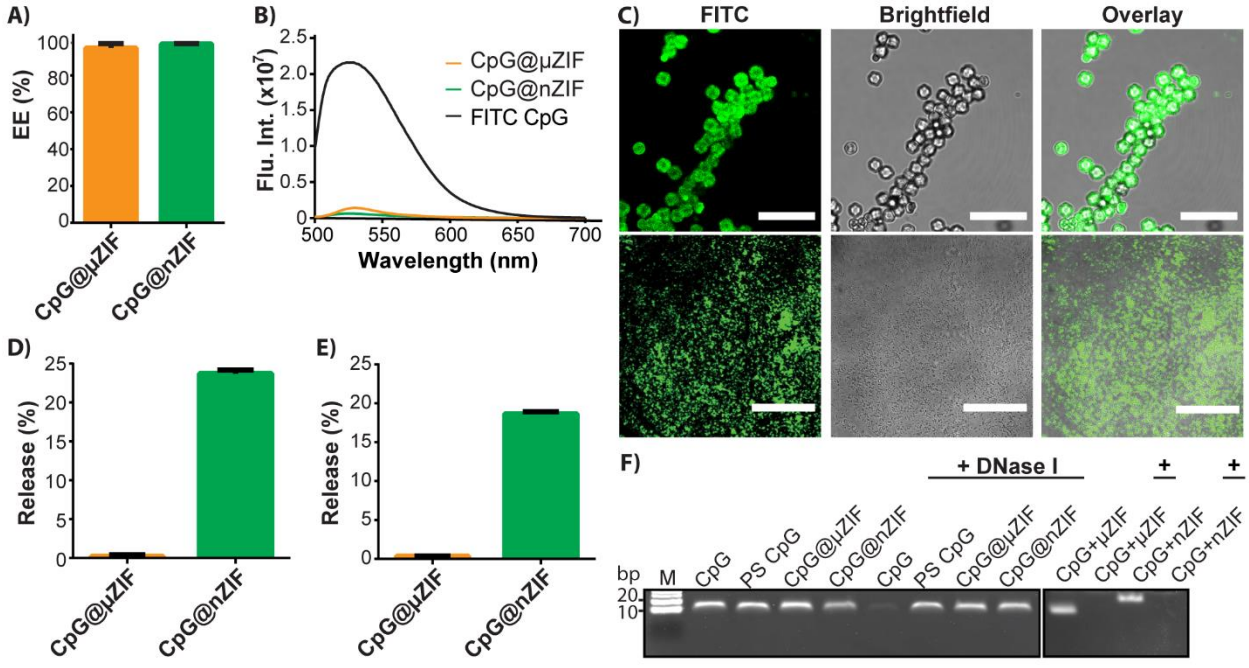

Figure 2. Characterization of CpG encapsulated in ZIF-8. A) Encapsulation efficiency of CpG in ZIF-8 as measured by fluorescence of the supernatant (n=3) (λ_{ex} = 495 nm; λ_{em} = 520 nm). B) Representative fluorescence spectra of the supernatant used to measure the encapsulation efficiency (λ_{ex} = 495 nm). C) Confocal images of FITC-labeled CpG@μZIF (top: scale bar = 10 μm) and CpG@nZIF (bottom: scale bar = 20 μm). D) Quantification of surface adsorbed CpG via a SDS wash and fluorescence measurement of the resulting supernatant (n=3) (λ_{ex} = 495 nm; λ_{em} = 520 nm). E) Quantification of surface adsorbed CpG via a DNase wash and fluorescence measurement of the resulting supernatant (n=3) (λ_{ex} = 495 nm; λ_{em} = 520 nm). F) 5% agarose gel characterizing the intactness of CpG before and after DNase I digestion to demonstrate the nuclease protection afforded by ZIF encapsulation.

With our nuclease resistant formulations of CpG, we then moved *in vitro*. First, we confirmed the biocompatibility of both formulations using an LDH cytotoxicity assay and RAW 264.7 murine macrophages (**Figure 3A**) where both formulations were found to be nontoxic after a 4 h incubation at the CpG concentrations we needed to use to induce B-cell maturation (3.3 μg/mL). We then moved forward with cellular assays using splenocytes prepared as a single cell suspension from spleens of naïve BALB/c mice. Splenocytes are a mixture of T-cells, B-cells, monocytes, granulocytes, dendritic cells, natural killer cells, and macrophages and are commonly used for *in vitro* immune stimulation experiments. Using FITC-labeled CpG, we were able to quantify the uptake of CpG@μZIF and CpG@nZIF by B-cells using flow cytometry. After incubating the CpG@ZIFs with splenocytes for 4 h, the cells were washed 3× with a low pH buffer to dissolve any surface ZIF.[46, 64-65] This ensured that the uptake observed indicated the degree of internalization of the particles. The cells were then stained with Alexa Fluor® 700 anti-mouse CD19 antibody to identify B-cells before being analyzed by flow. From these results, we

found that both CpG@ZIF formulations were able to improve the uptake of CpG (**Figure 3B&C**). We attribute this to the improved *in vitro* stability as well as the shielding of the strong negative charge of the DNA by the positively charged carrier. Furthermore, we found that the nano-sized formulation, CpG@nZIF, was taken up more efficiently as compared with the larger CpG@μZIF, following literature examples that nanoparticles are more optimized for cellular uptake. Following uptake by endocytosis, the ZIF is degraded by the acidic pH of the lysosome and releases the CpG cargo to activate B cells.[16, 44-45, 52, 66-68] To test this, we incubated CpG@μZIF and CpG@nZIF with splenocytes for 48 h, washed the cells with a low pH buffer, and subsequently stained the cells with three fluorescently-labeled antibodies that allow us to differentiate between naïve B-cells and activated B-cells — Alexa Fluor® 700 anti-mouse CD19 antibody, Alexa Fluor® 647 anti-mouse CD80 antibody, and PE anti-mouse CD86 antibody. In this study we employed PS CpG as a positive control and PS GpC, an antisense complement to PS CpG, as a negative control. Using flow cytometry, we were able to quantify B-cell activation where we found that both CpG@μZIF and CpG@nZIF were able to improve B-cell activation, even matching the performance of the "gold standard" PS CpG (**Figure 3D&E**). Curiously, despite the significantly enhanced uptake of the CpG@nZIF as compared to CpG@μZIF, there was no significant difference in B-cell activation in these two formulations.

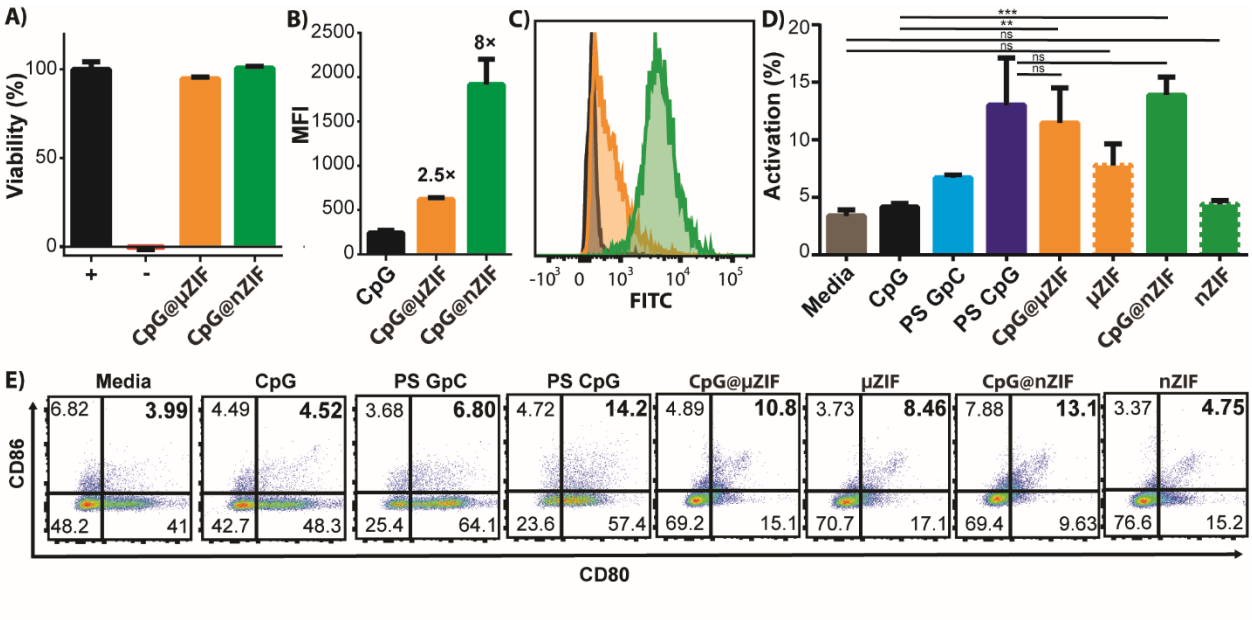

Figure 3. Evaluation of micro and nano CpG@ZIF *in vitro*. A) LDH cytotoxicity assay quantifying the biocompatibility of CpG@µZIF and CpG@nZIF with RAW 264.7 murine macrophages after 4 h (n=3). B) Uptake of FITC-labeled CpG@µZIF and CpG@nZIF by $CD19^+$ B-cells after 4 h incubation as measured by flow cytometry (n=3). C) Representative histogram of the uptake of FITC-labeled CpG, CpG@µZIF, and CpG@nZIF in $CD19^+$ B-cells. D) Percent of activated B-cells ($CD19^+$ $CD80^+$ $CD86^+$) after 48 h stimulation with CpG@µZIF and CpG@nZIF as measured by flow cytometry (n=3). E) Representative flow plots of B-cell activation by CpGs and CpG@ZIFs. Statistical significance was calculated by ordinary one-way ANOVA with Tukey's multiple comparison test (*$p < 0.05$, **$p < 0.01$, ***$p < 0.0005$, ****$p < 0.0001$; ns = not significant ($p > 0.05$)).

CONCLUSIONS

In this work, we demonstrate how the zinc-based MOF, ZIF-8, can be used to encapsulate the ssDNA immunoadjuvant CpG. By tuning the metal-to-ligand ratios, we were able to synthesize both micro and nano sizes of the encapsulated formulation. Encapsulation of CpG within ZIF-8

was shown to stabilize the phosphodiester nucleic acid by protecting it from nuclease degradation. Furthermore, encapsulation of the negatively charged biomacromolecule in the positively charged nanocarrier, ZIF-8, improved cellular uptake of the CpG in B-cells with nano significantly outperforming micro. Together these improvements have demonstrated that ZIF encapsulation has the potential to enhance the function of CpG in adjuvanting an immune response through the activation of B-cells to a comparable degree to the state-of-the-art PS CpG. From this work we hope to shed light on the prospect of using MOFs for the stabilization of phosphodiester DNAs.

AUTHOR INFORMATION

Corresponding Author

Jeremiah J. Gassensmith - Department of Chemistry and Biochemistry, The University of Texas at Dallas, 800 W. Campbell Road, Richardson, Texas 75080, United States; Department of Biomedical Engineering, The University of Texas at Dallas, 800 W. Campbell Road, Richardson, Texas 75080, United States; http://orcid.org/0000-0001-6400-8106; Email: gassensmith@utdallas.edu; Web: www.gassensmithlab.com

Author Contributions

O.R.B. optimized the synthesis of CpG@ZIFs and executed SEM, gel electrophoresis, and all *in vitro* studies. F. C. H. performed DLS and ζ potential characterizations. Y. W. performed PXRD characterizations. S. D. D. performed BET nitrogen isotherm experiments under the supervision of R. A. S.. R. E. performed confocal fluorescence microscopy, fluorimetry experiments, and aided in all *in vitro* studies. A. S. also performed fluorimetry experiments. A. R. aided in gel electrophoresis characterizations. O. R. B. and J. J. G. composed the manuscript. J. J. G.

conceived the project. All authors have read and given their approval to the final version of the manuscript.

Funding Sources

J.J.G. acknowledges National Science Foundation (Grants CAREER DMR-1654405 and DMR-2003534) and the Welch Foundation (Grant AT-1989-20190330).

Notes

The authors declare no competing interests.

REFERNCES

1. Liang, W.; Xu, H.; Carraro, F.; Maddigan, N. K.; Li, Q.; Bell, S. G.; Huang, D. M.; Tarzia, A.; Solomon, M. B.; Amenitsch, H.; Vaccari, L.; Sumby, C. J.; Falcaro, P.; Doonan, C. J., Enhanced Activity of Enzymes Encapsulated in Hydrophilic Metal–Organic Frameworks. *Journal of the American Chemical Society* **2019,** *141* (6), 2348-2355.

2. Wang, C.; Sudlow, G.; Wang, Z.; Cao, S.; Jiang, Q.; Neiner, A.; Morrissey, J. J.; Kharasch, E. D.; Achilefu, S.; Singamaneni, S., Metal-Organic Framework Encapsulation Preserves the Bioactivity of Protein Therapeutics. *Advanced Healthcare Materials* **2018,** *7* (22), 1800950.

3. Luzuriaga, M. A.; Welch, R. P.; Dharmarwardana, M.; Benjamin, C. E.; Li, S.; Shahrivarkevishahi, A.; Popal, S.; Tuong, L. H.; Creswell, C. T.; Gassensmith, J. J., Enhanced Stability and Controlled Delivery of MOF-Encapsulated Vaccines and Their Immunogenic Response In Vivo. *ACS Applied Materials & Interfaces* **2019,** *11* (10), 9740-9746.

4. Herbert, F. C.; Abeyrathna, S. S.; Abeyrathna, N. S.; Wijesundara, Y. H.; Brohlin, O. R.; Carraro, F.; Amenitsch, H.; Falcaro, P.; Luzuriaga, M. A.; Durand-Silva, A.; Diwakara, S. D.; Smaldone, R. A.; Meloni, G.; Gassensmith, J. J., Stabilization of supramolecular membrane protein–lipid bilayer assemblies through immobilization in a crystalline exoskeleton. *Nature Communications* **2021,** *12*, 2202.

5. Welch, R. P.; Lee, H.; Luzuriaga, M. A.; Brohlin, O. R.; Gassensmith, J. J., Protein–Polymer Delivery: Chemistry from the Cold Chain to the Clinic. *Bioconjugate Chemistry* **2018,** *29* (9), 2867-2883.

6. Luzuriaga, M. A.; Shahrivarkevishahi, A.; Herbert, F. C.; Wijesundara, Y. H.; Gassensmith, J. J., Biomaterials and nanomaterials for sustained release vaccine delivery. *WIREs Nanomedicine and Nanobiotechnology* **2021,** *13* (6), e1735.

7. Introduction to Metal–Organic Frameworks. *Chemical Reviews* **2012,** *112* (2), 673-674.

8. Zhou, H.-C. J.; Kitagawa, S., Metal–Organic Frameworks (MOFs). *Chemical Society Reviews* **2014,** *43* (16), 5415-5418.

9. Long, J. R.; Yaghi, O. M., The pervasive chemistry of metal–organic frameworks. *Chemical Society Reviews* **2009,** *38* (5), 1213-1214.

10. Ellis, J. E.; Zeng, Z.; Hwang, S. I.; Li, S.; Luo, T.-Y.; Burkert, S. C.; White, David L.; Rosi, N. L.; Gassensmith, J. J.; Star, A., Growth of ZIF-8 on molecularly ordered 2-methylimidazole/single-walled carbon nanotubes to form highly porous, electrically conductive composites. *Chemical Science* **2019,** *10* (3), 737-742.

11. Shi, L.; Wu, J.; Qiao, X.; Ha, Y.; Li, Y.; Peng, C.; Wu, R., In Situ Biomimetic Mineralization on ZIF-8 for Smart Drug Delivery. *ACS Biomaterials Science & Engineering* **2020,** *6* (8), 4595-4603.

12. Lyu, F.; Zhang, Y.; Zare, R. N.; Ge, J.; Liu, Z., One-Pot Synthesis of Protein-Embedded Metal–Organic Frameworks with Enhanced Biological Activities. *Nano Letters* **2014,** *14* (10), 5761-5765.

13. Liang, K.; Ricco, R.; Doherty, C. M.; Styles, M. J.; Bell, S.; Kirby, N.; Mudie, S.; Haylock, D.; Hill, A. J.; Doonan, C. J.; Falcaro, P., Biomimetic mineralization of metal-organic frameworks as protective coatings for biomacromolecules. *Nature Communications* **2015,** *6*, 7240.

14. Chen, Y.; Li, P.; Modica, J. A.; Drout, R. J.; Farha, O. K., Acid-Resistant Mesoporous Metal–Organic Framework toward Oral Insulin Delivery: Protein Encapsulation, Protection, and Release. *Journal of the American Chemical Society* **2018,** *140* (17), 5678-5681.

15. Zhou, Z.; Gao, Z.; Shen, H.; Li, M.; He, W.; Su, P.; Song, J.; Yang, Y., Metal–Organic Framework in Situ Post-Encapsulating DNA–Enzyme Composites on a Magnetic Carrier with High Stability and Reusability. *ACS Applied Materials & Interfaces* **2020,** *12* (6), 7510-7517.

16. Zhang, G.; Fu, X.; Sun, H.; Zhang, P.; Zhai, S.; Hao, J.; Cui, J.; Hu, M., Poly(ethylene glycol)-Mediated Assembly of Vaccine Particles to Improve Stability and Immunogenicity. *ACS Applied Materials & Interfaces* **2021,** *13* (12), 13978-13989.

17. Healy, C.; Patil, K. M.; Wilson, B. H.; Hermanspahn, L.; Harvey-Reid, N. C.; Howard, B. I.; Kleinjan, C.; Kolien, J.; Payet, F.; Telfer, S. G.; Kruger, P. E.; Bennett, T. D., The thermal stability of metal-organic frameworks. *Coordination Chemistry Reviews* **2020,** *419*, 213388.

18. Voskanyan, A. A.; Goncharov, V. G.; Novendra, N.; Guo, X.; Navrotsky, A., Thermodynamics Drives the Stability of the MOF-74 Family in Water. *ACS Omega* **2020,** *5* (22), 13158-13163.

19. Park, K. S.; Ni, Z.; Côté, A. P.; Choi, J. Y.; Huang, R.; Uribe-Romo, F. J.; Chae, H. K.; O'Keeffe, M.; Yaghi, O. M., Exceptional chemical and thermal stability of zeolitic imidazolate frameworks. *Proceedings of the National Academy of Sciences* **2006,** *103* (27), 10186-10191.

20. Li, S.; Dharmarwardana, M.; Welch, R. P.; Ren, Y.; Thompson, C. M.; Smaldone, R. A.; Gassensmith, J. J., Template-Directed Synthesis of Porous and Protective Core–Shell Bionanoparticles. *Angewandte Chemie International Edition* **2016,** *55* (36), 10691-10696.

21. Li, S.; Gassensmith, J. J., Synthesis of Metal–Organic Frameworks on Tobacco Mosaic Virus Templates. In *Protein Scaffolds: Design, Synthesis, and Applications*, Udit, A. K., Ed. Springer New York: New York, NY, 2018, Vol. 1798, pp 95-108.

22. Xiong, F.; Qin, Z.; Chen, H.; Lan, Q.; Wang, Z.; Lan, N.; Yang, Y.; Zheng, L.; Zhao, J.; Kai, D., pH-responsive and hyaluronic acid-functionalized metal–organic frameworks for therapy of osteoarthritis. *Journal of Nanobiotechnology* **2020,** *18*, 139.

23. He, L.; Liu, Y.; Lau, J.; Fan, W.; Li, Q.; Zhang, C.; Huang, P.; Chen, X., Recent progress in nanoscale metal-organic frameworks for drug release and cancer therapy. *Nanomedicine* **2019,** *14* (10), 1343-1365.

24. Luzuriaga, M. A.; Benjamin, C. E.; Gaertner, M. W.; Lee, H.; Herbert, F. C.; Mallick, S.; Gassensmith, J. J., ZIF-8 degrades in cell media, serum, and some—but not all—common laboratory buffers. *Supramolecular Chemistry* **2019,** *31* (8), 485-490.

25. Florindo, H. F.; Lopes, J.; Silva, L. C.; Corvo, M. L.; Martins, M. B.; Gaspar, R., Chapter Twenty One - Regulatory Development of Nanotechnology-Based Vaccines. In *Micro and Nanotechnology in Vaccine Development*, Skwarczynski, M.; Toth, I., Eds. William Andrew Publishing: 2017; pp 393-410.

26. Wang, Z.-B.; Xu, J., Better Adjuvants for Better Vaccines: Progress in Adjuvant Delivery Systems, Modifications, and Adjuvant-Antigen Codelivery. *Vaccines* **2020,** *8* (1), 128.

27. Abbasi, S.; Uchida, S., Multifunctional Immunoadjuvants for Use in Minimalist Nucleic Acid Vaccines. *Pharmaceutics* **2021,** *13* (5), 644.

28. Tizard, I. R., Adjuvants and adjuvanticity. *Vaccines for Veterinarians* **2021**, 75-86.e1.

29. Pulendran, B.; S. Arunachalam, P.; O'Hagan, D. T., Emerging concepts in the science of vaccine adjuvants. *Nature Reviews Drug Discovery* **2021,** *20*, 454-475.

30. Krieg, A. M.; Yi, A. K.; Matson, S.; Waldschmidt, T. J.; Bishop, G. A.; Teasdale, R.; Koretzky, G. A.; Klinman, D. M., CpG motifs in bacterial DNA trigger direct B-cell activation. *Nature* **1995,** *374* (6522), 546-549.

31. Fehér, K., Single Stranded DNA Immune Modulators with Unmethylated CpG Motifs: Structure and Molecular Recognition by Toll-Like Receptor 9. *Current Protein & Peptide Science* **2019,** *20* (11), 1060-1068.

32. Ishii, K. J.; Akira, S., Innate immune recognition of nucleic acids: Beyond toll-like receptors. *International Journal of Cancer* **2005,** *117* (4), 517-523.

33. Jabbari, K.; Bernardi, G., Cytosine methylation and CpG, TpG (CpA) and TpA frequencies. *Gene* **2004,** *333*, 143-149.

34. Bode, C.; Zhao, G.; Steinhagen, F.; Kinjo, T.; Klinman, D. M., CpG DNA as a vaccine adjuvant. *Expert Review of Vaccines* **2011,** *10* (4), 499-511.

35. Krug, A.; Rothenfusser, S.; Hornung, V.; Jahrsdörfer, B.; Blackwell, S.; Ballas, Z. K.; Endres, S.; Krieg, A. M.; Hartmann, G., Identification of CpG oligonucleotide sequences with high induction of IFN-alpha/beta in plasmacytoid dendritic cells. *European Journal of Immunology* **2001,** *31* (7), 2154-2163.

36. Hartmann, G.; Weeratna, R. D.; Ballas, Z. K.; Payette, P.; Blackwell, S.; Suparto, I.; Rasmussen, W. L.; Waldschmidt, M.; Sajuthi, D.; Purcell, R. H.; Davis, H. L.; Krieg, A. M., Delineation of a CpG phosphorothioate oligodeoxynucleotide for activating primate immune responses in vitro and in vivo. *Journal of Immunology* **2000,** *164* (3), 1617-1624.

37. Steinhagen, F.; Kinjo, T.; Bode, C.; Klinman, D. M., TLR-based immune adjuvants. *Vaccine* **2011,** *29* (17), 3341-3355.

38. Shirota, H.; Klinman, D. M., Chapter 9 - CpG Oligodeoxynucleotides as Adjuvants for Clinical Use. In *Immunopotentiators in Modern Vaccines (Second Edition)*, Schijns, V. E. J. C.; O'Hagan, D. T., Eds. Academic Press: 2017; pp 163-198.

39. van den Boorn, J. G.; Barchet, W.; Hartmann, G., Chapter 1 - Nucleic Acid Adjuvants: Toward an Educated Vaccine. In *Advances in Immunology*, Melief, C. J. M., Ed. Academic Press: 2012; Vol. 114, pp 1-32.

40. Senti, G.; Johansen, P.; Haug, S.; Bull, C.; Gottschaller, C.; Müller, P.; Pfister, T.; Maurer, P.; Bachmann, M. F.; Graf, N.; Kündig, T. M., Use of A-type CpG oligodeoxynucleotides as an adjuvant in allergen-specific immunotherapy in humans: a phase I/IIa clinical trial. *Clinical & Experimental Allergy* **2009,** *39* (4), 562-570.

41. Mutwiri, G. K.; Nichani, A. K.; Babiuk, S.; Babiuk, L. A., Strategies for enhancing the immunostimulatory effects of CpG oligodeoxynucleotides. *Journal of Controlled Release* **2004,** *97* (1), 1-17.

42. Hager, S.; Fittler, F. J.; Wagner, E.; Bros, M., Nucleic Acid-Based Approaches for Tumor Therapy. *Cells* **2020,** *9* (9), 2061.

43. Pohar, J.; Lainšček, D.; Kunšek, A.; Cajnko, M.-M.; Jerala, R.; Benčina, M., Phosphodiester backbone of the CpG motif within immunostimulatory oligodeoxynucleotides augments activation of Toll-like receptor 9. *Scientific Reports* **2017,** *7*, 14598.

44. Zhang, Y.; Wang, F.; Ju, E.; Liu, Z.; Chen, Z.; Ren, J.; Qu, X., Metal-Organic-Framework-Based Vaccine Platforms for Enhanced Systemic Immune and Memory Response. *Advanced Functional Materials* **2016,** *26* (35), 6454-6461.

45. Poddar, A.; Conesa, J. J.; Liang, K.; Dhakal, S.; Reineck, P.; Bryant, G.; Pereiro, E.; Ricco, R.; Amenitsch, H.; Doonan, C.; Mulet, X.; Doherty, C. M.; Falcaro, P.; Shukla, R., Encapsulation, Visualization and Expression of Genes with Biomimetically Mineralized Zeolitic Imidazolate Framework-8 (ZIF-8). *Small* **2019,** *15* (36), 1902268.

46. Luzuriaga, M. A.; Herbert, F. C.; Brohlin, O. R.; Gadhvi, J.; Howlett, T.; Shahrivarkevishahi, A.; Wijesundara, Y. H.; Venkitapathi, S.; Veera, K.; Ehrman, R.; Benjamin, C. E.; Popal, S.; Burton, M. D.; Ingersoll, M. A.; De Nisco, N. J.; Gassensmith, J. J., Metal-Organic Framework Encapsulated Whole-Cell Vaccines Enhance Humoral Immunity against Bacterial Infection. *ACS Nano* **2021,** *15* (11*)*, 17426–17438.

47. Li, S.; Zhou, X.; Chen, Z.; Herbert, F. C.; Jayawickramage, R.; Panangala, S. D.; Luzuriaga, M. A.; Alahakoon, S. B.; Diwakara, S. D.; Meng, X.; Fei, L.; Ferraris, J.; Smaldone, R. A.; Gassensmith, J. J., Hierarchical Porous Carbon Arising from Metal–Organic Framework-Encapsulated Bacteria and Its Energy Storage Potential. *ACS Applied Materials & Interfaces* **2020,** *12* (10), 11884-11889.

48. Hou, X.; Zaks, T.; Langer, R.; Dong, Y., Lipid nanoparticles for mRNA delivery. *Nature Reviews Materials* **2021,** *6*, 1078-1094.

49. Donaldson, B.; Lateef, Z.; Walker, G. F.; Young, S. L.; Ward, V. K., Virus-like particle vaccines: immunology and formulation for clinical translation. *Expert Review of Vaccines* **2018,** *17* (9), 833-849.

50. Chang, H.-I.; Yeh, M.-K., Clinical development of liposome-based drugs: formulation, characterization, and therapeutic efficacy. *International Journal of Nanomedicine* **2012,** *7*, 49-60.

51. Chen, T.-T.; Yi, J.-T.; Zhao, Y.-Y.; Chu, X., Biomineralized Metal–Organic Framework Nanoparticles Enable Intracellular Delivery and Endo-Lysosomal Release of Native Active Proteins. *Journal of the American Chemical Society* **2018,** *140* (31), 9912-9920.

52. Zhang, H.; Chen, W.; Gong, K.; Chen, J., Nanoscale Zeolitic Imidazolate Framework-8 as Efficient Vehicles for Enhanced Delivery of CpG Oligodeoxynucleotides. *ACS Applied Materials & Interfaces* **2017,** *9* (37), 31519-31525.

53. Lee, B. K.; Yun, Y.; Park, K., PLA micro- and nano-particles. *Advanced Drug Delivery Reviews* **2016,** *107*, 176-191.

54. Silva, A. L.; Soema, P. C.; Slütter, B.; Ossendorp, F.; Jiskoot, W., PLGA particulate delivery systems for subunit vaccines: Linking particle properties to immunogenicity. *Human Vaccines & Immunotherapeutics* **2016,** *12* (4), 1056-1069.

55. Sousa de Almeida, M.; Susnik, E.; Drasler, B.; Taladriz-Blanco, P.; Petri-Fink, A.; Rothen-Rutishauser, B., Understanding nanoparticle endocytosis to improve targeting strategies in nanomedicine. *Chemical Society Reviews* **2021,** *50* (9), 5397-5434.

56. Yeung, T.; Gilbert, G. E.; Shi, J.; Silvius, J.; Kapus, A.; Grinstein, S., Membrane Phosphatidylserine Regulates Surface Charge and Protein Localization. *Science* **2008,** *319* (5860), 210-213.

57. Ma, Y.; Poole, K.; Goyette, J.; Gaus, K., Introducing Membrane Charge and Membrane Potential to T Cell Signaling. *Frontiers in Immunology* **2017,** *8* (1513).

58. Li, S.; Dharmarwardana, M.; Welch, R. P.; Benjamin, C. E.; Shamir, A. M.; Nielsen, S. O.; Gassensmith, J. J., *ACS Applied Materials & Interfaces* **2018**, *10* (21), 18161–18169.

59. Wang, Y.; Zhang, N.; Tan, D.; Qi, Z.; Wu, C., Facile Synthesis of Enzyme-Embedded Metal–Organic Frameworks for Size-Selective Biocatalysis in Organic Solvent. *Frontiers in Bioengineering and Biotechnology* **2020,** *8* (714).

60. Ricco, R.; Wied, P.; Nidetzky, B.; Amenitsch, H.; Falcaro, P., Magnetically responsive horseradish peroxidase@ZIF-8 for biocatalysis. *Chemical Communications* **2020,** *56* (43), 5775-5778.

61. Liang, K.; Richardson, J. J.; Cui, J.; Caruso, F.; Doonan, C. J.; Falcaro, P., Metal–Organic Framework Coatings as Cytoprotective Exoskeletons for Living Cells. *Advanced Materials* **2016,** *28* (36), 7910-7914.

62. Sun, C.; Chang, L.; Hou, K.; Liu, S.; Tang, Z., Encapsulation of live cells by metal-organic frameworks for viability protection. *Science China Materials* **2019,** *62* (6), 885-891.

63. Yan, S.; Zeng, X.; Wang, Y.; Liu, B.-F., Biomineralization of Bacteria by a Metal–Organic Framework for Therapeutic Delivery. *Advanced Healthcare Materials* **2020,** *9* (12), 2000046.

64. Galeotti, C.; Karnam, A.; Das, M.; Kaveri, S. V.; Bayry, J., Acid Stripping of Surface IgE Antibodies Bound to FcεRI Is Unsuitable for the Functional Assays That Require Long-Term Culture of Basophils and Entire Removal of Surface IgE. *International Journal of Molecular Sciences* **2020,** *21* (2), 510.

65. Kameyama, S.; Horie, M.; Kikuchi, T.; Omura, T.; Tadokoro, A.; Takeuchi, T.; Nakase, I.; Sugiura, Y.; Futaki, S., Acid wash in determining cellular uptake of Fab/cell-permeating peptide conjugates. *Peptide Science* **2007,** *88* (2), 98-107.

66. Sun, C.-Y.; Qin, C.; Wang, X.-L.; Yang, G.-S; Shao, K.-Z.; Lan, Y.-Q.; Su, Z.-M.; Huang, P.; Wang, C.-G.; Wang, E.-B., Zeolitic imidazolate framework-8 as efficient pH-sensitive drug delivery vehicle. *Dalton Transactions* **2012**, *41* (23), 6906-6909.

67. Zhong, X.; Sun, X., Nanomedicines based on nanoscale metal-organic frameworks for cancer immunotherapy. *Acta Pharmacol Sin* **2020**, *41*, 928–935.

68. Abdelhamid, H. N.; Dowaidar, M.; Hällbrink, M.; Langel, Ü., Gene delivery using cell penetrating peptides-zeolitic imidazolate frameworks. *Microporous and Mesoporous Materials* **2020**, *300*, 110173.